Steel and Composite Structures, *Vol. 31, No. 5 (2019) 489-502*
DOI: https://doi.org/10.12989/scs.2019.31.5.489

Free and forced analysis of perforated beams

Alaa A. Abdelrahman [1a], Mohamed A. Eltaher [*2,3],
Abdallah M. Kabeel [1b], Azza M. Abdraboh [4c] and Asmaa A. Hendi [5d]

[1] *Mechanical Design & Production Department, Faculty of Engineering, Zagazig University, P.O. Box 44519, Zagazig, Egypt*
[2] *Mechanical Engineering Department, Faculty of Engineering, King Abdulaziz University, P.O. Box 80204, Jeddah, Saudi Arabia*
[3] *Mechanical Design & Production Department, Faculty of Engineering, Zagazig University, P.O. Box 44519, Zagazig, Egypt*
[4] *Physics Department, Faculty of Science, Banha University, Banha, Egypt*
[5] *Physics Department, Faculty of Science, University of Jeddah,P.O.Box 80327, Jeddah, Saudi Arabia*

(*Received January 28, 2019, Revised March 19, 2019, Accepted March 26, 2019*)

Abstract. This article presents a unified mathematical model to investigate free and forced vibration responses of perforated thin and thick beams. Analytical models of the equivalent geometrical and material characteristics for regularly squared perforated beam are developed. Because of the shear deformation regime increasing in perforated structures, the investigation of dynamical behaviors of these structures becomes more complicated and effects of rotary inertia and shear deformation should be considered. So, both Euler-Bernoulli and Timoshenko beam theories are proposed for thin and short (thick) beams, respectively. Mathematical closed forms for the eigenvalues and the corresponding eigenvectors as well as the forced vibration time response are derived. The validity of the developed analytical procedure is verified by comparing the obtained results with both analytical and numerical analyses and good agreement is detected. Numerical studies are presented to illustrate effects of beam slenderness ratio, filling ratio, as well as the number of holes on the dynamic behavior of perforated beams. The obtained results and concluding remarks are helpful in mechanical design and industrial applications of large devices and small systems (MEMS) based on perforated structure.

Keywords: resonant frequencies; forced Vibration, perforated beam; dynamical behavior; filling ratio; semi-analytical method

1. Introduction

Beam structure is extensively used in real application, ranging from macro-structures (i.e., aerospace, civil, marine, mechanical and nuclear structures), to micro-structures (i.e., actuators, resonators, microphone, switches, and RF MEMS) to nano-structures (i.e., atomic force microscope, nanoprobes, nanoactuators, nanosensors, and nanoswitches). During service life, beams may be subjected to various types of dynamic loading. Thus, safe and reliable design of beams requires accurate analysis of their dynamical behaviors, such as, internal characteristics (natural frequencies) and overall behaviors (responses).

Nikkhoo *et al*. (2007) studied dynamic behavior and modal control of an Euler–Bernoulli beam under the effect of moving mass with different number of controlled modes and actuators. Adhikary *et al*. (2012) investigated dynamic behavior of reinforced concrete beams under varying rates of concentrated loading by using an explicit finite element program LS-DYNA. Bouremana *et al*. (2013) presented a new first-order shear deformation beam theory based on neutral surface position for bending and free vibration analysis of functionally graded beams. Eltaher *et al*. (2013, 2014a, b) studied free vibration of thin and thick nanobeams by using finite element method. Bennai *et al*. (2015) and Bourada *et al*. (2015) developed a new refined hyperbolic shear and normal deformation beam theory to study the free vibration and buckling of functionally graded (FG) sandwich beams. Eltaher *et al*. (2016) implemented higher-order shear deformation beam theories to investigate the effects of thermal load and shear force on the buckling of nanobeams. Tekili *et al*. (2017) studied free and forced vibration of aluminum beams strengthened by carbon/epoxy composite under the action of moving loads at a constant speed. Bebiano *et al*. (2017) presented and illustrated the application of a semi-analytical Generalised Beam Theory (GBT) formulation for the dynamic analysis of high-speed railway bridge decks. Katariya and Panda (2018) presented numerical evaluation of transient deflection and frequency responses of sandwich shell structure using higher order theory and different mechanical loadings. Rajasekaran (2018) Analyzed axially functionally graded nano-tapered Timoshenko beams by element-based Bernstein pseudospectral collocation.

Sınır *et al*. (2018) exploited perturbation method and differential quadrature method to investigate nonlinear free and forced vibrations of axially functionally graded Euler-Bernoulli beams with non-uniform cross-section. Thai *et al*.

*Corresponding author, Professor,
E-mail: meltaher@kau.edu.sa; mmeltaher@zu.edu.eg
[a] Ph.D., E-mail: alaaabouahmed@gmail.com
[b] Ph.D., E-mail: amkabeel@zu.edu.eg
[c] Ph.D., E-mail: aza.abdrabo@fsc.bu.edu.eg
[d] Ph.D., E-mail: Ahendi@kau.edu.sa

ISSN: 1229-9367 (Print), 1598-6233 (Online)

(2018) proposed a simple beam theory accounting for shear deformation effects with one unknown for static bending and free vibration analysis of isotropic nanobeams. Driz *et al*. (2018) presented a novel higher shear deformation theory (HSDT) for bending, buckling and free vibration investigations of isotropic and functionally graded (FG) sandwich plates. Rouhi *et al*. (2019) illustrated nonlinear free and forced vibration of Timoshenko nanobeams based on Mindlin's second strain gradient theory. Gul *et al*. (2019) studied dynamics of a functionally graded beam were studied using Timoshenko and Euler-Bernoulli beam theories considering new spectrums. Greco *et al*. (2019) studied the inverse problem related to the identification of the flexural stiffness of an Euler Bernoulli beam to reconstruct its profile starting from available response data by using genetic algorithm.

Nowadays, perforation in various structures is necessary in design process due to technological reasons, such as, in the heat exchangers and nuclear power plants applications (Jeong and Amabili 2006), and in ships and offshore structures, (Kim *et al*. 2015). In micro/nano-structures, perforation is often necessary for sacrificial-layer removal, representing a technological constraint for the designer, De Pasquale *et al*. (2019). In 1996, Pedersen *et al*. (1996) predicted the in plane stiffness behavior and resonance frequency of beam-based MEMS resonant sensors by using finite difference method. Berggren *et al*. (2003) modeled the properties of regularly periodic holed structures materials by equivalent anisotropic materials. Jeong and Amabili (2006) studied natural frequencies and the corresponding mode shapes of perforated beams, whose lower surfaces contacted with an ideal liquid by using Rayleigh–Ritz method. Luschi and Pieri (2012) introduced closed forms for equivalent bending stiffness in the filled and the perforated sections of perforated beam to examine bending properties of beams with regular rectangular perforations. Tu *et al*. (2013) presented effects of etching holes on complementary metal oxide semiconductor–capacitive structure by the use of ANSYS simulation. Luschi and Pieri (2014) presented closed expressions for geometrical properties of perforated beam with periodic square to investigate resonance frequencies of slender perforated beam. Guha *et al*. (2015) presented general analytical model of capacitance of non-uniform meander based RF MEMS shunt switch with perforated structure incorporating fringing field effects. Luschi and Pieri (2016) developed analytical models to determine the resonance frequency of Lamé-mode resonators with a square grid of square perforations. Lee (2016) illustrated the effect of leakage on the sound absorption of a nonlinear perforated panel backed by a cavity.

She *et al*. (2017) investigated thermal buckling and postbuckling behaviors of functionally graded materials (FGM) beams based on Euler–Bernoulli, Timoshenko and various higher-order shear deformation beam theories. Ghayesh *et al*. (2017) examined the forced nonlinear size-dependent vibrations and bending of axially functionally graded tapered microbeams incorporating extensibility. Guha *et al*. (2017, 2018) presented a new method for design, modelling and optimization of a uniform MEMS shunt capacitive switch with perforation on upper beam to improve the Pull-in Voltage performance. Abdelbari *et al*. (2018) presented Single variable shear deformation model for bending analysis of thick beams. Shafiei and She (2018) studied vibration characteristics of two dimensional functionally graded (2D-FG) tubes based on higher order theory in the thermal environment. Heidari *et al*. (2018) developed numerical study for vibration response of concrete beams reinforced by nanoparticles. Bending, buckling and free vibration behaviors of perforated nonlocal nanobeams has been investigated by Eltaher *et al*. (2018a, b), according to Euler-Bernoulli and Timoshenko beam theories with nonlocal differential form of Eringen model. They found that, the size-scale and perforation parameters such as, perforation size and number of cutouts, have significant influences on static and dynamic behavior of nanobeams. She *et al*. (2018a) studied thermal buckling and post-buckling behaviors of functionally graded materials (FGM) tubes subjected to a uniform temperature rise and resting on elastic foundations via a refined beam model. She *et al*. (2018b) predicted wave propagation behaviors of functionally graded materials (FG) porous nanobeams based on Reddy’s higher-order shear deformation beam theory in conjunction with the non-local strain gradient theory. Kerid *et al*. (2019) investigated the magnetic field, thermal loads and small scale effects on the dynamic behaviors of perforated nanobeams with periodic square networks. Cortés *et al*. (2019) developed geometry simplification of open‑cell porous materials for elastic deformation by using finite element analysis.

According to the authors’ knowledge, no researchers have attempted to study free and forced vibration responses of perforated Euler and Timoshenko beams. Thus, the present work aims to fill this gap. So, this article presents closed form solutions for resonant frequencies, Eigen mode functions, and the forced vibration response for both perforated Euler-Bernoulli and Timoshenko beams. Mixed Galerkin-Laplace technique is exploited. Numerical studies show the significant effects of size and number of cutouts on the free and forced behaviors of perforated beam. The manuscript is arranged as follows: in Section 2, equivalent geometrical parameters, relative bending and shear stiffnesses, relative mass and rotary inertia are presented. Section 3 presents the mathematical formulation and governing equations for perforated beams. Solution methodology and closed forms for resonant frequencies, Eigen mode functions, and the forced vibration are derived in Section 4. The validation with previous respectable work is proved in Section 5. Section 6 is devoted to numerical results and parametric studies. Finally, at the end conclusions are summarized and listed in Section 7.

2. Geometric model of perforated beams

In order to keep efficient investigation of the dynamic behavior of perforated structures, the structure periodicity of the cut out holes should be considered. This section is devoted to present analytical closed forms for the equivalent geometrical and material characteristics of perforated

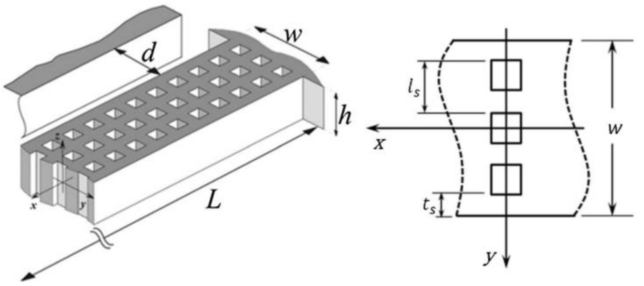

Fig. 1 Geometry of a perforated beam (Luschi and Pieri 2014)

beams. Perforated beam shown in Fig. 1, has a total length L, thickness h, width w, with a pattern of square holes of spatial period l_s , side $l_s - t_s$, and number of holes along the section are N. The ratio of the spatial period, t_s to the period length, l_s refers to the beam filling ratio, α which can be expressed as follows

$$\alpha = \frac{t_s}{l_s} \qquad 0 \leq \alpha \leq 1, \qquad\qquad (1)$$
$$\alpha = \begin{cases} 0 & \text{Fully perforated} \quad (Artificial\ case) \\ 1 & \text{Fully filled} \end{cases}$$

2.1 Relative bending stiffness ratio

Assume that, the total induced stress along the cross section for both fully filled solid beam and perforated one are equal, (Luschi and Pieri 2014, Eltaher *et al*. 2018a, b). Also, the stress distribution throughout the filled segment of the perforated beam is assumed to be linear and continuous. Based on these assumption, the relative bending stiffness ratio of the perforated beam to that of the solid one can be expressed as, Luschi and Pieri (2014)

$$\frac{(EI)_{eq}}{EI} = \left\{\frac{\alpha(N+1)(N^2+2N+\alpha^2)}{(1-\alpha^2+\alpha^3)N^3+3\alpha N^2+(3+2\alpha-3\alpha^2+\alpha^3)\alpha^2 N+\alpha^3}\right\} \qquad (2)$$

where, E is the elasticity modulus of the fully filled beam material, I is the second moment of area of the fully filled beam.

The dependency of the relative bending stiffness ratio, $[EI_{eq}/EI]$ is illustrated in Fig. 2. It is noticed that the relative bending stiffness increases with increasing the filling ratio due to the decrease in the hole size. On the other hand, increasing the number of holes at fixed filling ratio results in decreasing the relative bending stiffness. This is due to increasing the cut out positions with smaller size which results in decreasing the bulk material. Moreover, as the filling ratio approaches unity; ($\alpha > 0.8$), the relative bending stiffness approaches unity and an insignificant effect of the number of holes on the relative bending stiffness is noticed.

2.2 Relative shear stiffness ratio

Due to the perforation process, the cross-sections of the beam and its principal axis are no longer orthogonal so the shear deformations are not negligible even for slender beams. Assume that the unit cell is centered in the hole, the relative shear stiffness ratio of the perforated beam to that of the fully solid one can be given by, Luschi and Pieri (2014)

$$\frac{(GA)_{eq}}{GA} = \left(\frac{(1+N)\alpha^3}{2N}\right) \qquad (3)$$

where, E and G are the elasticity and shear moduli of the fully filled beam material, A is the sectional area of the fully filled beam.

Variations of the relative equivalent shear stiffness of the perforated beam to that of the solid beam, $[(GA)_{eq}/GA]$ with both filling ratio and the number of holes are presented in Fig. 3. It is seen that the relative shear stiffness increases with increasing the filling ratio i.e., decreasing the hole size while it is decreasing with increasing the number of holes. Additionally, for $N > 1$, the number of holes has insignificant effect on the relative shear stiffneas for filling ratios less than 0.5. Moreover, the equivalent resistance of the perforated beam to shear deformation is almost zero for filling ratios below 0.3. Thus, values of the filling ratios below 0.3 are not recommended in the design of perforated beam structures.

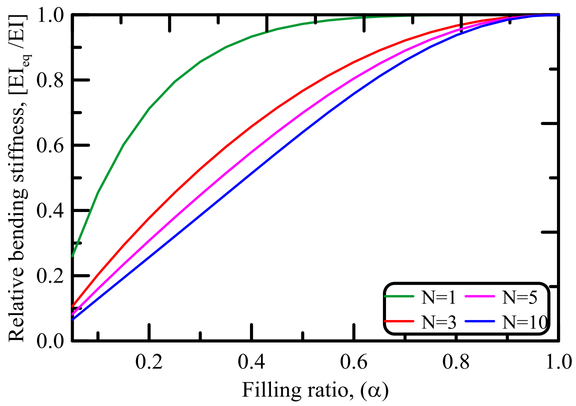

Fig. 2 Variation of the relative bending stiffness with the filling ratio at different number of holes

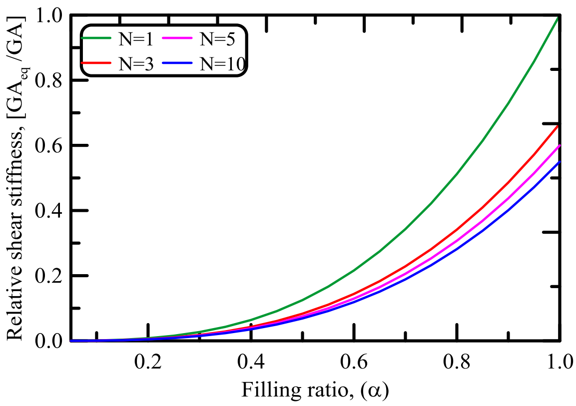

Fig. 3 Variation of the relative shear stiffness with the filling ratio at different number of holes

2.3 Relative mass per unit length ratio

The relative ratio of the equivalent mass per unit length of the perforated beam to that of the fully filled one can be expressed as, Eltaher *et al*. (2018a, b)

$$\frac{(\rho A)_{eq}}{\rho A} = \left\{\frac{[1 - N(\alpha - 2)]\alpha}{N + \alpha}\right\} \tag{4}$$

The nonlinear variation of the relative ratio of mass per unit length of the perforated beam to that of the fully filled one for different number of holes is depicted in Fig. 4. It may be noticed that the relative ratio of the mass per unit length increases with increasing the beam filling ratio while it is slightly decreasing with increasing the number of holes. For $N > 1$ and filling ratio $\alpha > 0.75$, the number of holes has no effect on the relative ratio of the mass per unit length.

2.4 Relative rotary inertia ratio

The relative ratio of the equivalent mass per unit length of the perforated beam to that of the fully filled one can be expressed as, Eltaher *et al*. (2018a, b)

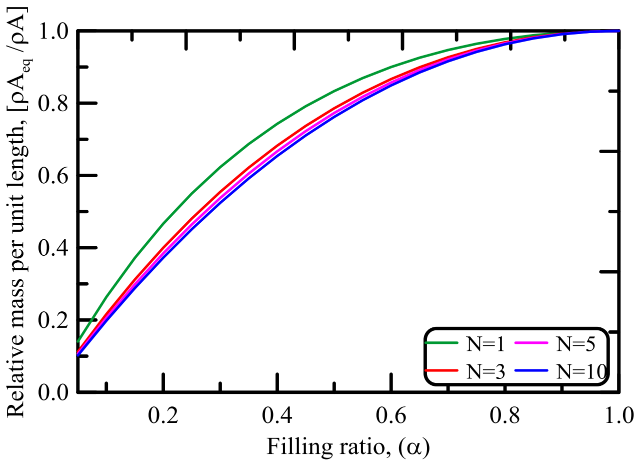

Fig. 4 Variation of the relative mass per unit length with the filling ratio at different number of holes

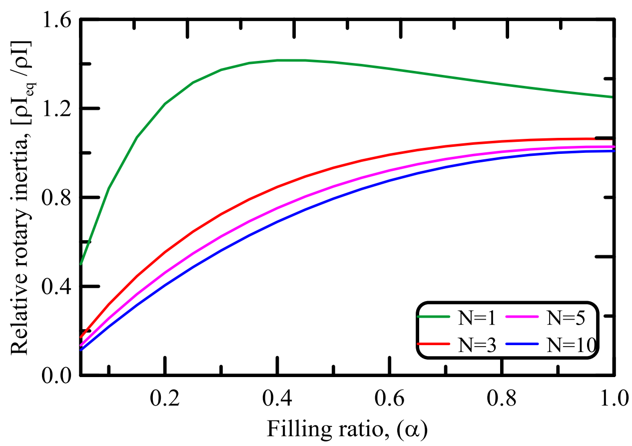

Fig. 5 Variation of the relative rotary inertia with the filling ratio at different number of holes

$$\frac{(\rho I)_{eq}}{\rho I} = \left\{\frac{\alpha[(2 - \alpha)N^3 + 3N^2 - 2(\alpha - 3)(\alpha^2 - \alpha + 1)N + \alpha^2 + 1]}{(N + \alpha)^3}\right\} \tag{5}$$

The nonlinear variation of the relative rotary inertia ratio with the filling ratio at different number of holes is illustrated in Fig. 5. It is seen that the relative rotary inertia ratio increases with increasing the beam filing ratio, i.e., decreasing the size of holes thus due to increasing the bulk material of the beam. In addition, it is decreasing with increasing the number of holes at a constant filling ratio this due to increasing the cut out positions with smaller sizes.

3. Mathematical formulations of perforated beams

3.1 Euler Bernoulli beam theory (*EBBT*)

The Euler–Bernoulli beam theory is based on that plane sections perpendicular to the axis of the beam before deformation remain plane, and rotate such that they remain perpendicular to the (deformed) axis after deformation Eltaher *et al*. (2012). Based on these assumptions, the axial and lateral displacements of a point located at a position (x, z) in the deformed configuration are given by

$$u(x,z,t) = -z\frac{\partial w(x,t)}{\partial x}, \qquad w(x,z,t) = w(x,t) \tag{6}$$

where u and w are the axial and lateral displacements of the midplane, respectively. Assuming small-strain, the strain displacement relations can be written as

$$\varepsilon_{xx} = \frac{\partial u(x,z,t)}{\partial x} = -z\frac{\partial^2 w(x,t)}{\partial x^2} \quad \text{and} \quad \gamma_{xz} = \frac{\partial w(x,z,t)}{\partial x} + \frac{\partial u(x,z,t)}{\partial z} = 0 \tag{7}$$

Considering linear isotropic homogenous elastic materials, the constitutive law can be written as

$$\sigma_{xx} = -Ez\frac{\partial^2 w(x,t)}{\partial x^2} \quad \text{and} \quad \tau_{xz} = G\,\gamma_{xz} = 0 \tag{8}$$

The strain energy for the perforated Euler Bernoulli beam (PEBB) can be expressed by the following equation

$$\pi = \frac{1}{2}\iiint_V \left(\sigma_{xx}\varepsilon_{xx} + \frac{1}{2}\tau_{xz}\gamma_{xz}\right) dV = \frac{1}{2}\int_0^l K_b \left(\frac{\partial^2 w(x,t)}{\partial x^2}\right)^2 dx \tag{9}$$

where $K_b = (EI)_{eq}$ is the equivalent bending stiffness of the perforated beam defined in Eq. (2). The kinetic energy of the fully filled solid beam is given by, Inman (2014)

$$T=\frac{1}{2}\int_0^l\left[\iint_A\left\{\rho\left[\frac{\partial}{\partial t}\left(-z\frac{\partial w(x,t)}{\partial x}\right)\right]^2+\rho\left(\frac{\partial w(x,t)}{\partial t}\right)^2\right\}dA\right]dx$$
$$=\frac{1}{2}\int_0^l\left\{\iint_A\rho\left[\frac{\partial}{\partial t}\left(-z\frac{\partial w(x,t)}{\partial x}\right)\right]^2dA+\iint_A\rho\left(\frac{\partial w(x,t)}{\partial t}\right)^2dA\right\}dx \quad (10)$$

Simplifying Eq. (10), the kinetic energy for PEBB can be written as

$$T=\frac{1}{2}\left\{\int_0^l I_1\left(\frac{\partial^2 w(x,t)}{\partial x\partial t}\right)^2dx+\int_0^l I_0\left(\frac{\partial w(x,t)}{\partial t}\right)^2dx\right\} \quad (11)$$

where $I_1=(\rho I)_{eq}$ and $I_0=(\rho A)_{eq}$ refer to the equivalent rotary inertia and the equivalent mass per unit length, respectively presented by Eqs. (4) and (5). Assuming that the beam is subjected to a distributed transverse load, $f(x, t)$, then the work done by the external distributed transverse is given by

$$W=\int_0^l f(x,t)\,w(x,t)\,dx \quad (12)$$

The dynamic equation of motion with the associated boundary conditions can be obtained by applying the generalized Hamilton's principle as

$$\delta\int_{t_1}^{t_2}(\pi-T-W)\,dt=0 \quad (13)$$

Substituting from Eqs. (9), (11) and (12) into Eq. (13) the dynamic equilibrium equation of motion of PEBB can be written as

$$I_0\frac{\partial^2 w(x,t)}{\partial t^2}-I_1\frac{\partial^4 w(x,t)}{\partial x^2\partial t^2}+K_b\left(\frac{\partial^4 w(x,t)}{\partial x^4}\right)=f(x,t) \quad (14)$$

3.2 Timoshenko beam theory (TBT)

The displacement field of the Timoshenko beam theory for pure bending is written as

$$u(x,y,z,t)=-z\varphi(x,t),\qquad v(x,y,z,t)=0 \quad \text{and} \quad w(x,y,z,t)=w(x,t) \quad (15)$$

where u, v, and w refer to the components of displacement in x, y, and z directions, respectively. Assuming small strain, the corresponding kinematic relations can be expressed as

$$\varepsilon_{xx}=-z\frac{\partial\varphi(x,t)}{\partial x} \quad \text{and} \quad \gamma_{xz}=\frac{\partial w(x,t)}{\partial x}-\varphi(x,t) \quad (16)$$

The constitutive equations is given by

$$\sigma_{xx}=-Ez\frac{\partial\varphi(x,t)}{\partial x} \quad \text{and} \quad \sigma_{xz}=\kappa G\,\gamma_{xz}=G\kappa\left(\frac{\partial w(x,t)}{\partial x}-\varphi(x,t)\right) \quad (17)$$

where κ is the shear correction factor. The strain energy for the perforated Timoshenko beam (PTB) can be expressed as

$$\pi=\frac{1}{2}\iiint_V(\sigma_{xx}\varepsilon_{xx}+\sigma_{xz}\gamma_{xz})dV=\frac{1}{2}\int_0^l\left\{K_b\left(\frac{\partial\varphi(x,t)}{\partial x}\right)^2+K_s\left(\frac{\partial w(x,t)}{\partial x}-\varphi(x,t)\right)^2\right\}dx \quad (18)$$

where K_b and $K_s=\kappa(GA)_{eq}$ are the equivalent bending and shear stiffness of the PTB, respectively, as defined in Eqs. (2) and (3). The kinetic energy of the fully filled solid beam is given by, Kim *et al*. (2017).

$$T=\frac{1}{2}\int_0^l\left[\iint_A\left\{\rho\left[-z\frac{\partial\varphi(x,t)}{\partial t}\right]^2+\rho\left(\frac{\partial w(x,t)}{\partial t}\right)^2\right\}dA\right]dx$$
$$=\frac{1}{2}\int_0^l\left\{\iint_A\rho z^2\left(\frac{\partial\varphi(x,t)}{\partial t}\right)^2+\iint_A\rho\left(\frac{\partial w(x,t)}{\partial t}\right)^2dA\right\}dx \quad (19)$$

Simplifying Eq. (19), the kinetic energy for PTB can be written as

$$T=\frac{1}{2}\left\{\int_0^l I_1\left(\frac{\partial\varphi(x,t)}{\partial t}\right)^2dx+\int_0^l I_0\left(\frac{\partial w(x,t)}{\partial t}\right)^2dx\right\} \quad (20)$$

The work done by the external distributed transverse loads, $f(x, t)$ and $M(x, t)$ is given by

$$W=\int_0^l f(x,t)\,w(x,t)+M(x,t)\,\varphi(x,t)\,dx \quad (21)$$

The dynamic equation of motion with the associated boundary conditions can be obtained by applying the generalized Hamilton's principle as

$$\delta\int_{t_1}^{t_2}(\pi-T-W)\,dt=0 \quad (22)$$

Substituting from Eqs. (18) to (22) and evaluating the integral, the dynamic equations of motion based on TBT can be written as

$$I_0 \frac{\partial^2 w(x,t)}{\partial t^2} - K_s \left[\frac{\partial^2 w(x,t)}{\partial x^2} - \frac{\partial \varphi(x,t)}{\partial x}\right] = f(x,t) \quad (23a)$$

$$I_1 \frac{\partial^2 \varphi(x,t)}{\partial t^2} - K_s \left[\frac{\partial w(x,t)}{\partial x} - \varphi(x,t)\right] - K_b \frac{\partial^2 \varphi(x,t)}{\partial x^2} = M(x,t) \quad (23b)$$

Differentiating Eq. (23b) w.r.t. x and substituting from Eq. (23a) for the value of $\frac{\partial \varphi(x,t)}{\partial x}$, the coupled equations can be reduced to one single equation. Thus one can write

$$\begin{aligned} &K_b \frac{\partial^4 w(x,t)}{\partial x^4} - \left(I_1 + \frac{K_b I_0}{K_s}\right) \frac{\partial^4 w(x,t)}{\partial t^2 \partial x^2} \\ &+ I_0 \frac{\partial^2 w(x,t)}{\partial t^2} + \frac{I_1 I_0}{K_s} \frac{\partial^4 w(x,t)}{\partial t^4} \\ &= -M(x,t) + \left(f(x,t) + \frac{I_1}{K_s} \frac{\partial^2 f(x,t)}{\partial t^2} - \frac{K_b}{K_s} \frac{\partial^2 f(x,t)}{\partial x^2}\right) \end{aligned} \quad (24)$$

4. Solution methodology

This section is devoted to present closed forms for the resonant frequencies and the forced vibration time response for perforated beams.

4.1 Free vibration

4.1.1 Perforated Euler Bernoulli beam (PEBB)

Considering free vibration analysis, the governing equation of motion of (PEBB) can be written as

$$I_0 \frac{\partial^2 w(x,t)}{\partial t^2} - I_1 \frac{\partial^4 w(x,t)}{\partial x^2 \partial t^2} + K_b \left(\frac{\partial^4 w(x,t)}{\partial x^4}\right) = 0 \quad (25)$$

The free vibration response can be expressed as

$$w(x,t) = W(x) \exp(i\omega t) \quad (26)$$

where $W(x)$ is the Eigen mode shape function (eigenvector) and ω is the natural frequency (eigenvalue) of vibration. Substitute from Eq. (26) into Eq. (25) yields

$$[-\omega^2 I_0 \, W(x) + I_1 \omega^2 \, W''(x) + K_b \, W''''(x)] \exp(i\omega t) = 0 \quad (27)$$

Eq. (27) can be expressed as

$$\{K_b \, D^{(4)} - I_1 \omega^2 \, D^{(2)} - \omega^2 I_0\} W(x) \exp(i\omega t) = 0 \quad (28)$$

The general solution of Eq. (28) can be written as

$$\begin{aligned} W(x) &= C_1 \cos(D_1 x) + C_2 \sin(D_1 x) \\ &+ C_3 \cosh(D_2 x) + C_4 \sinh(D_2 x) \end{aligned} \quad (29)$$

Considering the simply supported beam, the following boundary conditions are imposed

$$\begin{aligned} W(x)|_{x=0} &= W(x)|_{x=L} \\ &= W''(x)|_{x=0} = W''(x)|_{x=L} = 0 \end{aligned} \quad (30)$$

Substituting with Eq. (30) into Eq. (29), the natural frequency can be expressed as

$$\omega_n^2 = \frac{\left(\frac{n\pi}{L}\right)^4 \left(\frac{K_b}{I_0}\right)}{1 + \left(\frac{I_1}{I_0}\right)\left(\frac{n\pi}{L}\right)^2}, \qquad n = 1, 2, 3, \ldots\ldots\ldots\ldots..\infty \quad (31)$$

4.1.2 Perforated Timoshenko beam (PTB)

By the same way, the resonant frequencies and the mode shapes can be obtained for PTB. The dynamic equation of motion of (PTB) for the free vibration analysis is written as

$$\begin{aligned} &K_b \frac{\partial^4 w(x,t)}{\partial x^4} - \left(I_1 + \frac{K_b I_0}{K_s}\right) \frac{\partial^4 w(x,t)}{\partial t^2 \partial x^2} \\ &+ I_0 \frac{\partial^2 w(x,t)}{\partial t^2} + \frac{I_1 I_0}{K_s} \frac{\partial^4 w(x,t)}{\partial t^4} = 0 \end{aligned} \quad (32)$$

The free vibration response can be expressed as

$$\begin{aligned} w(x,t) &= W(x) \exp(i\omega t) \quad \text{and} \\ \varphi(x,t) &= \Phi(x) \exp(i\omega t) \end{aligned} \quad (33)$$

where $W(x)$ is the Eigen mode shape function (eigenvector) and ω is the natural frequency (eigenvalue) of vibration. Substitute from Eq. (33) into Eq. (32) yields

$$\left[\frac{I_1 I_0}{K_s} \omega^4 \, W(x) - I_0 \omega^2 \, W(x) + \left\{I_1 + \frac{K_b I_0}{K_s}\right\} \omega^2 \, W''(x) - + K_b \, W''''(x)\right] \exp(i\omega t) = 0 \quad (34)$$

Eq. (34) can be expressed as

$$\left[K_b \, D^{(4)} - \left\{I_1 + \frac{I_0 K_b}{K_s}\right\} \omega^2 \, D^{(2)} - I_0 \omega^2 + \frac{\omega^4 I_0 I_1}{K_s}\right] W(x) \exp(i\omega t) = 0 \quad (35)$$

The general solution of Eq. (35) can be written as

$$\begin{aligned} W(x) &= C_1 \cos(D_1 x) + C_2 \sin(D_1 x) \\ &+ C_3 \cosh(D_2 x) + C_4 \sinh(D_2 x) \end{aligned} \quad (36)$$

Considering the simply supported beam, the following boundary conditions are imposed

$$\begin{aligned} W(x)|_{x=0} &= W(x)|_{x=L} = W''(x)|_{x=0} \\ &= W''(x)|_{x=L} = 0 \end{aligned} \quad (37)$$

Substituting with Eq. (37) into Eq. (36), Considering the bending deformation mode (BDM), the natural frequencies can be expressed as

$$(\omega_n^2)_{BDM} = \left[\left\{\frac{K_b}{2I_1}+\frac{K_s}{2I_0}\right\}\left(\frac{n\pi}{L}\right)^2+\frac{K_s}{2I_1}\right] - \sqrt{\left[\left\{\frac{K_b}{2I_1}+\frac{K_s}{2I_0}\right\}\left(\frac{n\pi}{L}\right)^2+\frac{K_s}{2I_1}\right]^2 - 4\left(\frac{K_b}{2I_1}\right)\left(\frac{K_s}{2I_0}\right)\left(\frac{n\pi}{L}\right)^4} \quad (38a)$$

On the other hand, the natural frequencies for the shear deformation mode (SDM) can be written as

$$(\omega_n^2)_{SDM} = \left[\left\{\frac{K_b}{2I_1}+\frac{K_s}{2I_0}\right\}\left(\frac{n\pi}{L}\right)^2+\frac{K_s}{2I_1}\right] + \sqrt{\left[\left\{\frac{K_b}{2I_1}+\frac{K_s}{2I_0}\right\}\left(\frac{n\pi}{L}\right)^2+\frac{K_s}{2I_1}\right]^2 - 4\left(\frac{K_b}{2I_1}\right)\left(\frac{K_s}{2I_0}\right)\left(\frac{n\pi}{L}\right)^4} \quad (38b)$$

Neglecting the effect of rotary inertia, the natural frequencies can be expressed as

$$\omega_n = \left(\frac{\frac{K_b}{I_0}\left(\frac{n\pi}{L}\right)^4}{1+\frac{K_b}{K_s}\left(\frac{n\pi}{L}\right)^2}\right)^{1/2}, \quad n = 1, 2, 3, \ldots\ldots\infty \quad (39)$$

4.2 Forced vibration response using mixed Galerkin Laplace technique

4.2.1 Forced vibration response of (*PEBBT*)

Consider a simply supported beam with length L, width b and thickness h. the beam is subjected to a uniformly distributed load with intensity $\bar{P}$. The mixed Galerkin-Laplace technique is adopted to obtain the time response of the forced vibration of perforated beams. In this technique, the spatial dependency of the forced vibration response is detected by the Galerkin technique while the time dependency is obtained by the Laplace and inverse Laplace techniques. Consequently, the forced vibration time response is expressed by a series of two separate multiplied functions, the first function is a spatially dependent function and must satisfies all boundary conditions while the second is a time dependent one and must satisfies all initial conditions. The transverse deflection function can be expressed in the form

$$w_n(x,t) = \sum_{j=1}^{n} T_j(t) W_j(x) \quad (40)$$

where $W_j(x)$ is the j-th shape function which satisfy all the boundary conditions and $T_j(t)$ is the corresponding time dependent amplitude which satisfy the initial conditions. The shape functions are chosen to be linearly independent, orthonormal and must satisfy all boundary condition for the convergence of Galerkin method.

$$\int_0^L W_i(x) W_j(x)\,dx = \delta_{ij} \quad (41)$$

where δ_{ij} is the kroners delta. Although w_n satisfies the boundary conditions, it generally, does not satisfy equation (14). Substitute from Eq. (40) into (14) the residual function can be expressed as

$$\bar{R}_n(x,t) = I_0\left(\sum_{i=1}^{n} \ddot{T}_i(t) W_i(x)\right) - I_1\left(\sum_{i=1}^{n} \ddot{T}_i(t) W_i^{(2)}(x)\right) + K_b\left(\sum_{i=1}^{n} T_i(t) W_i^{(4)}(x)\right) - \bar{P} \quad (42)$$

The shape function that satisfies all boundary and the normal modes orthogonality conditions can be expressed as

$$W_i(x) = \sqrt{\frac{2}{L}}\sin\left(\frac{i\pi x}{l}\right) \quad (43a)$$

Then the derivatives of the shape function can be expressed as

$$W_i^{(2)}(x) = -\lambda_i W_i(x) \text{ and } W_i^{(4)}(x) = (\lambda_i)^2 W_i(x), \quad \lambda_i = \left(\frac{i\pi}{l}\right)^2, \quad i = 1,2,\ldots\ldots\ldots,n \quad (43b)$$

To the satisfy the orthogonality conditions required for the Galerkin technique, the following relations should be verified

$$\iint_\Omega \bar{R}_n(x,t) W_i(x)\,dx\,dt = 0, \quad i = 1,2,\ldots.,n \quad (44)$$

where $\Omega = [0, l]\times[0, t]$. This leads to n equations verified by the functions $T_j(t)$

$$\int_0^t\int_0^l \left(I_0\left(\sum_{i=1}^{n} \ddot{T}_j(t) W_j(x)\right) - I_1\left(\sum_{i=1}^{n} \ddot{T}_j(t) W_j^{(2)}(x)\right) + K_b\left(\sum_{i=1}^{n} T_j(t) W_j^{(4)}(x)\right) - \bar{P}\right) W_i(x)\,dx\,dt = 0 \quad (45)$$

Using Eq. (41), Eq. (45) can be rewritten as

$$[I_0 + I_1(\lambda_j)]\ddot{T}_j(t) + (\lambda_j)^2 K_b T_j(t) = \int_0^L \bar{P}\, W_j(x)\,dx = \bar{p}\left(\sqrt{\frac{2}{L}}\times\frac{L}{j\pi}\right)(1-cos(j\pi)) \quad (46)$$

Eq. (46) can be rewritten as

$$\ddot{T}_j(t) + \frac{(\lambda_j)^2 K_b}{[I_0 + I_1(\lambda_j)]} T_j(t) = \frac{1}{[I_0 + I_1(\lambda_j)]}\int_0^L \bar{P}\, W_j(x)\,dx = \frac{\bar{p}\left(\sqrt{\frac{2}{L}}\times\frac{L}{j\pi}\right)}{[I_0 + I_1(\lambda_j)]}(1-cos(j\pi)) = P_j \quad (4)$$

with

$$P_j = \frac{\bar{p}\left(\sqrt{\frac{2}{L}} \times \frac{L}{j\pi}\right)}{\left[I_0 + I_1(\lambda_j)\right]}\left(1 - cos(j\pi)\right) \quad (47b)$$

Using the Laplace transform techniques and the initial conditions

$$\left.\frac{d^k T_j(t)}{dt^k}\right|_{t=0} = \int_0^L \frac{\partial^k w(x,0)}{\partial t^k} W_j(x)dx\,, \quad k = 0, 1, 2, \dots\dots \quad (47c)$$

The functions $T_j(t)$ are determined independent of one another as

$$T_j(t) = \frac{\bar{p}\left(\sqrt{\frac{2}{L}} \times \frac{L}{j\pi}\right)}{\left(\lambda_j\right)^2 K_b}\left(1 - cos(j\pi)\right)\left(1 - cos\left(\beta_j t\right)\right) \quad (48a)$$

The elastodynamic transverse deflection throughout the PEBB span can be given by

$$w_n(x,t) = \sum_{j=1}^{n} \alpha_j sin(\frac{j\pi x}{L})\left(1 - cos\left(\beta_j t\right)\right) \quad (48b)$$

with

$$\alpha_j = \frac{\bar{p}\sqrt{\frac{2}{L}}\left(\sqrt{\frac{2}{L}} \times \frac{L}{j\pi}\right)}{\left(\lambda_j\right)^2 K_b}\left(1 - cos(j\pi)\right) \quad \text{and}$$

$$\beta_j = \left(\frac{\left(\lambda_j\right)^2 K_b}{\left[I_0 + I_1(\lambda_j)\right]}\right)^{1/2} \quad (48c)$$

Using Eqs. (48), the relation for the residual can be obtained to check the equilibrium equation versus the number of terms used to express the dynamic response of PBs.

4.2.2 Forced vibration response of (PTBT)

Neglecting the effect of the rotary inertia, the residual function of Eq. (24) can be expressed as

$$\begin{aligned}\bar{R}_n(x,t) = \sum_{i=1}^{n} I_0 \frac{d^2 T_i(t)}{dt^2} W_i(x) \\ - \frac{I_0 K_b}{K_s}\left(\sum_{i=1}^{n} \ddot{T}_i(t) W_i^{(2)}(x)\right) \\ + K_b\left(\sum_{i=1}^{n} T_i(t) W_i^{(4)}(x)\right) - \bar{P}\end{aligned} \quad (49)$$

Considering the simply supported beam, the shape function that satisfies all boundary conditions and its derivatives are written as expressed in Eqs. (43). To satisfy the orthogonality conditions of the residual function as

$$\iint_{\Omega} \bar{R}_n(x,t) W_i(x) dx dt = 0\,, \quad i = 1,2, \dots, n \quad (50)$$

where $\Omega = [0, l] \times [0, t]$. This leads to n equations verified by the functions $T_j(t)$

$$\begin{aligned}\int_0^t \int_0^l \Bigg(\sum_{i=1}^{n} I_0 \frac{d^2 T_j(t)}{dt^2} W_j(x) \\ - \frac{I_0 K_b}{K_s}\left(\sum_{i=1}^{n} \frac{d^2 T_j(t)}{dt^2} W_j^{(2)}(x)\right) \\ + K_b\left(\sum_{i=1}^{n} T_j(t) W_j^{(4)}(x)\right) \\ - \bar{P}\Bigg) W_i(x) dx dt = 0\end{aligned} \quad (51)$$

Using Eq. (43), Eq. (51) can be rewritten as

$$\begin{aligned}\frac{d^2 T_j(t)}{dt^2} + \eta_j^2\, T_j(t) \\ = \left\{\frac{1}{I_0\left\{1 + \left(\frac{K_b}{K_s}\right)\left(\lambda_j\right)\right\}}\right\}\int_0^L \bar{P}\, W_j(x)dx = P_j\end{aligned} \quad (52a)$$

with

$$P_j = \left\{\frac{\bar{p}\left(\sqrt{\frac{2}{L}} \times \frac{L}{j\pi}\right)}{I_0\left\{1 + \left(\frac{K_b}{K_s}\right)\left(\lambda_j\right)\right\}}\right\}\left(1 - cos(j\pi)\right) \quad \text{and}$$

$$\eta_j^2 = \frac{\left(\lambda_j\right)^2 K_b}{I_0\left\{1 + \left(\frac{K_b}{K_s}\right)\left(\lambda_j\right)\right\}} \quad (52b)$$

Using the Laplace transform techniques and the initial conditions

$$\left.\frac{d^k T_j(t)}{dt^k}\right|_{t=0} = \int_0^L \frac{\partial^k w(x,0)}{\partial t^k} W_j(x)dx, \quad k = 0, 1, 2, \dots\dots \quad (53)$$

The functions $T_j(t)$ are determined independent of one another.

$$T_j(t) = \left\{\frac{\bar{p}\left(\sqrt{\frac{2}{L}} \times \frac{L}{j\pi}\right)}{\left(\lambda_j\right)^2 K_b}\right\}\left(1 - cos(j\pi)\right)\left(1 - cos\left(\eta_j t\right)\right) \quad (54a)$$

Finally, an approximate closed form describing the dynamic transverse deflection throughout the PTB span can be expresses as

$$w_n(x,t) = \sum_{j=1}^{n} \Lambda_j sin(\frac{j\pi x}{L})\left(1 - cos\left(\eta_j t\right)\right) \quad (54b)$$

with

$$\Lambda_j = \left\{\frac{\bar{p}\sqrt{\frac{2}{L}}\left(\sqrt{\frac{2}{L}} \times \frac{L}{j\pi}\right)}{\left(\lambda_j\right)^2 K_b}\right\}\left(1 - cos(j\pi)\right) \quad \text{and}$$

$$\eta_j = \left(\frac{\left(\lambda_j\right)^2 K_b}{I_0\left\{1 + \left(\frac{K_b}{K_s}\right)\left(\lambda_j\right)\right\}}\right)^{1/2} \quad (54c)$$

Using Eqs. (54), an expression for the residual can be obtained to check the equilibrium equation for the considered number of terms in the closed form solution.

5. Numerical results

This section is keen mainly to two subsections. The first subsection is devoted to validate the proposed analytical procedure for analyzing the dynamic behavior of perforated beams. The resonant frequencies of a simply supported Timoshenko solid beam are compared with analytical and numerical results presented by Song *et al*. (2016).

The second subsection is devoted to study and analyze the free and forced transverse vibration behaviors of perforated beams considering both PEBBT and PTBT. Beams with different (h/L) ratios are considered to investigate the shear deformation effect due to the perforation process. Effects of beam filling ratio as well as the number of holes on the dynamic behavior of perforated beams are investigated for each case. Through this subsection, consider a simply supported beam with L = 1 m, cross sectional area, $A = w*h$, the moment of inertia $I = (wh^3/12)$. The beam is subjected to a uniformly distributed load of intensity 75 N/m, which is applied suddenly at $t = 0$ and then maintained constant. The beam is made of steel with mass density, ρ = 7860 kg/m^3 and modulus of elasticity, E = 210 GPa and modulus of rigidity, G = 81 Gpa. The dynamic behavior is investigated considering four values of %(h/L) ratio; h/L = 1%, 2%, 8%, and 20%. In all cases the beam length and width are kept constant; L = 1 m and w = 0.02 m.

5.1 Validation of uniform solid Timoshenko beam

Consider a simply supported uniform solid Timoshenko beam with the following material and geometric properties: Modulus of elasticity, E = 202 GPa, modulus of rigidity, G = 77.7 GPa, mass density, ρ = 15267 kg/m^3, length, L = 4.352 m, cross sectional area, $A = 1.31\times10^{-3}$ m^2, the second moment of area, $I = 5.71\times10^{-7}$ m^4, the shear correction factor, k = 0.7. Song *et al*. (2016) analyzed the same problem analytically by the exact and spectral element method (SEM) and numerically using the finite element (FEM). The developed analytical methodology is applied to detect the circular frequencies of the problem for the two case with and without the rotary inertia (RI). The obtained natural circular frequencies are listed in Table 1. It is noticed that good agreement is noticed between the obtained values of the natural frequencies are and that obtained by Song *et al*. (2016) with maximum relative error of 2.52% at the 10th mode. Additionally, insignificant effect of the rotary inertia on the resonant frequencies is noticed for the lowest fifth modes while only 1.2% drop in the circular frequency due to the rotary inertia effect is detected at the 10th mode.

5.2 Free vibration analysis

Through this section, effects of both filling ratio and the number of holes on the nondimensional resonant frequencies of the perforated beams are investigated. The nondimensional frequency can be defined as

$$\varpi_n = \omega_n \left(L^2 \sqrt{\frac{\rho A}{EI}} \right) \tag{55}$$

Table 1 Natural circular frequencies for solid uniform Timoshenko beam (Hz)

Mode	Present study		Song *et al*. (2016)			% Error
	With RI	Without RI	Exact	SEM	FEM	
1	6.295	6.296	6.3	6.3	6.3	0.0635
2	25.136	25.150	25.18	25.18	25.18	0.11915
3	56.398	56.469	56.61	56.61	56.61	0.2491
4	99.873	100.094	100.52	100.52	100.52	0.4238
5	155.281	155.808	156.85	156.85	156.85	0.6643
10	597.447	604.622	620.28	620.28	620.28	2.5243

The dependency of the nondimensional resonant frequencies, ϖ_n on the beam filing ratios and the number of holes for the first lowest fifth modes for both stocky and slender beams are depicted in Figs. 6-13. It is noticed that, for all values of %R, except for the case of N = 1 for PEBB, the nondimensional resonant frequencies are increasing with increasing the beam filling ratio due to the decreasing in the hole size and consequently increasing the beam equivalent stiffness. On the other hand, these nondimensional resonant frequencies are decreasing with increasing the number of holes at constant beam filling ratio because of increasing the cutout positions with smaller sizes which decreases the beam equivalent stiffness. It is also noticed that, for all values of %R, due the shear deformation effect smaller values of the nondimensional resonant frequencies are predicted by PTBT compared to that obtained by PEBBT in which the shear deformation effect is neglected.

Considering the beam height to length ratio, %R = %(h/L) it is noticed that, at smaller values of %R, large deviations between the nondimensional resonant frequencies predicted by EBBT and that obtained by TBT,

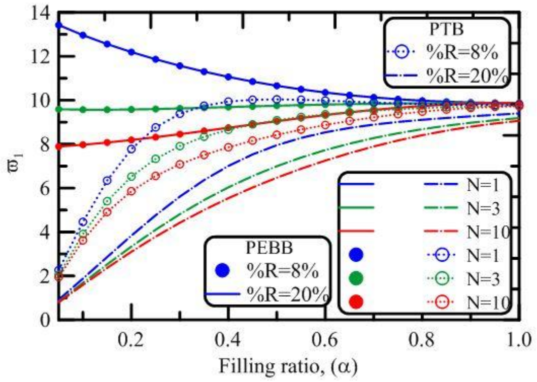

Fig. 6 Variation of ϖ_1 with the filling ratio for both PEBB and PTB at different number of holes for %R = 8% and 20%

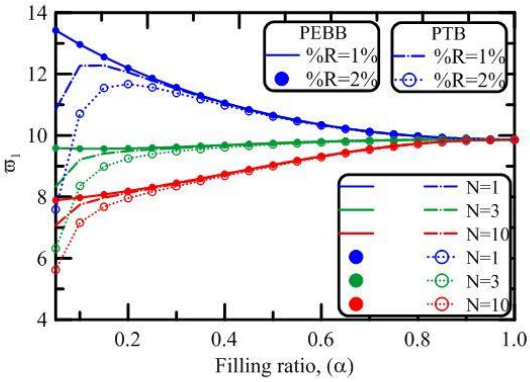

Fig. 7 Variation of ϖ_1 with the filling ratio for both PEBB and PTB at different number of holes for %R = 1% and 2%

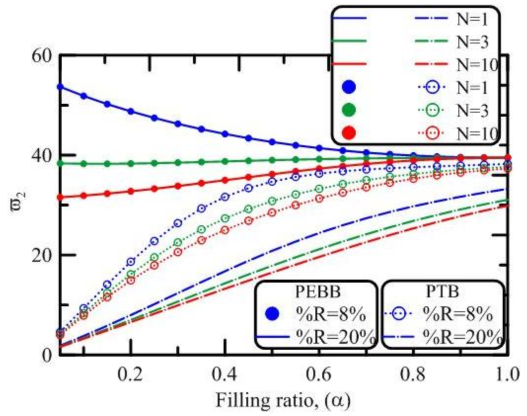

Fig. 8 Variation of ϖ_2 with the filling ratio for both PEBB and PTB at different number of holes for %R = 8% and 20%

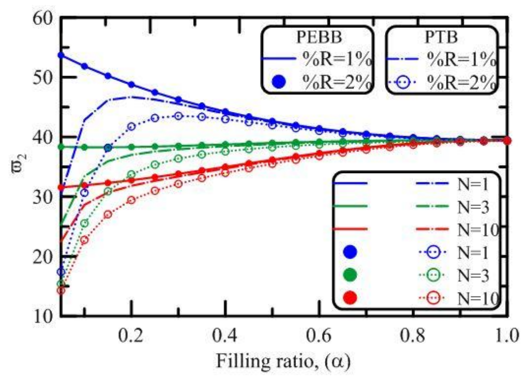

Fig. 9 Variation of ϖ_2 with the filling ratio for both PEBB and PTB at different number of holes for %R = 1% and 2%

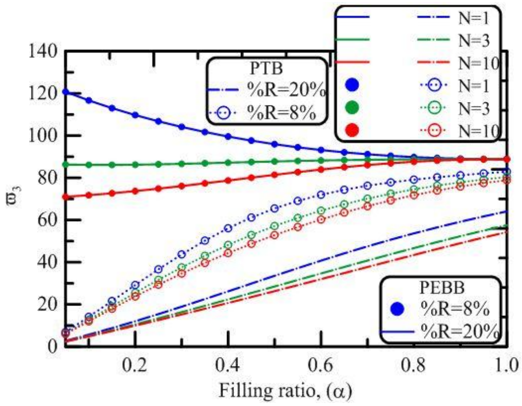

Fig. 10 Variation of ϖ_3 with the filling ratio for both PEBB and PTB at different number of holes for %R = 8% and 20%

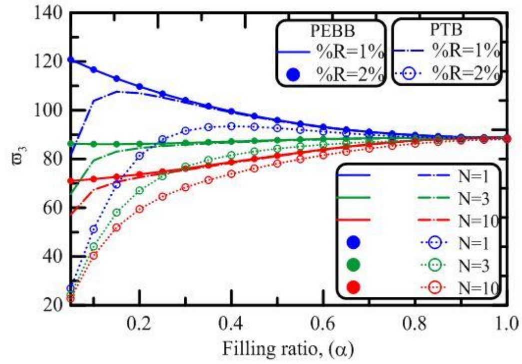

Fig. 11 Variation of ϖ_3 with the filling ratio for both PEBB and PTB at different number of holes for %R = 1% and 2%

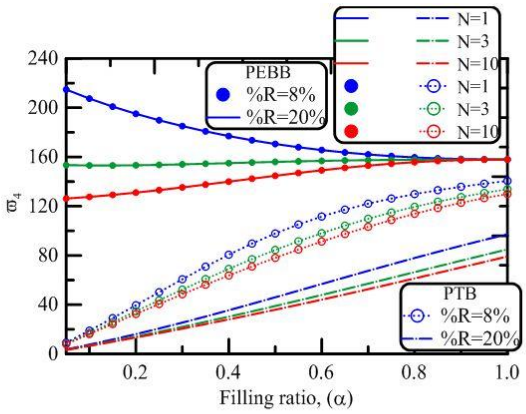

Fig. 12 Variation of ϖ_4 with the filling ratio for both PEBB and PTB at different number of holes for %R = 8% and 20%

consequently, the EBBT can't efficiently predict the resonant frequencies of perforated beams within this range of filling ratio for all number of holes. For relative height to length ratio, %R = 1% both PTBT and PEBBT predict almost the same values fffpor the nondimensional resonant frequencies for the first lowest forth modes for all values of filling ratios greater than 0.3. Thus, EBBT can be employed to investigate the resonant frequencies of PBs with %R = 1% in the perforation range having $\alpha \geq 0.3$. Increasing this ratio results in decreasing the perforation applicability zone of EBBT to predict the dynamic behaviors of PBs.

It is also seen that for stocky perforated beams with %R of 8%, small deviation between the 1st resonant frequency predicted by EBBT and that obtained TBT for $\alpha \geq 0.5$ for all number of holes. This deviation is increasing with increasing

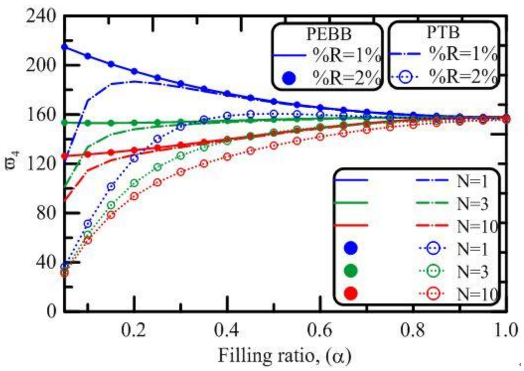

Fig. 13 Variation of ϖ_4 with the filling ratio for both PEBB and PTB at different number of holes for %R = 1% and 2%

the vibration modes. At higher values of %R = 20%, large deviations between the nondimensional resonant frequencies obtained from PEBB and the predicted by PTB even for the 1st mode.

5.3 Forced vibration response

In this section, the forced time response of a simply supported perforated beam under a uniformly distributed time constant load having an intensity of 75 N/m is investigated. To check the applicability of the simplest EBBT to investigate the transient response of perforated beams, beam with two different values of %R (2% and 20%) using both EBBT and TBT. One thousand terms are considered in the residual equation to satisfy the equilibrium dynamic equation of motion with relative error percentage of 0.063%. Effects of the beam filling ratio, the number of holes as well as the beam slenderness ratio on the transient time response of perforated beams are investigated.

The time dependency of the forced vibration response of PEBB and PTB at different filling ratios and different number of holes for both stocky and slender beams are illustrated in Figs. 14-19. Generally, it is noticed that almost the same quantitative values of the maximum transverse deflection are predicted by both PEBB and the corresponding PTB for both stocky and slender beams for all values of filling ratios and number of holes. On the other hand, it may be noticed that, the filling ratio has a significant effect on both amplitude and the phase shift of the forced vibration time response of both PEBB and the corresponding PTB. As the beam filling ratio increases, the forced vibration amplitude decreases due to decreasing the hole size which results in decreasing the system flexibility. Moreover the peaks values of these amplitudes are shifted to right with increasing the filling ratio. On the other hand, increasing the number of holes results in increasing the maximum transverse deflection due to increasing the cut out positions which increases the system flexibility. The reciprocal of the beam slenderness ratio, %R significantly affects the transient time response for both PEBB and PTB. Increasing the relative percentage ratio, %R results in decreasing the maximum transverse deflection. As depicted from Figs. 14-19, the ratio of the transvers deflection

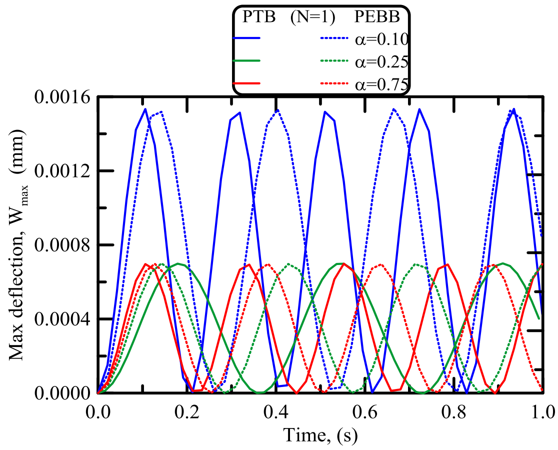

Fig. 14 Variation of W_{max} with the filling ratio for stocky PBs with %R = 20% at N = 1

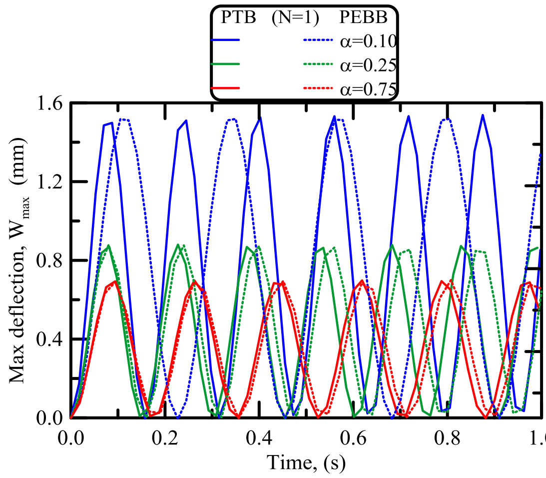

Fig. 15 Variation of W_{max} with the filling ratio for slender PBs with %R = 2% at N = 1

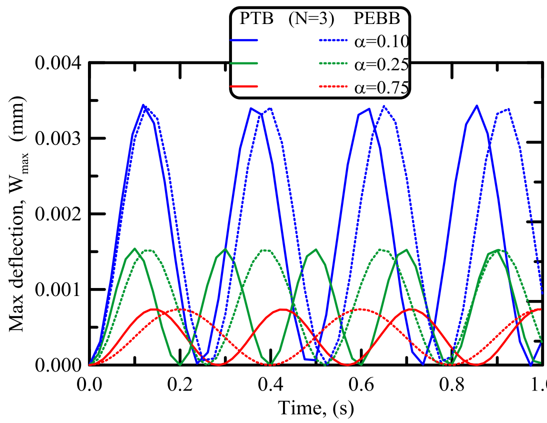

Fig. 16 Variation of W_{max} with the filling ratio for stocky PBs with %R = 20% at N = 3

obtained from %R = 2% to that obtained from %R = 20% is almost one thousands due to the decrease in the system flexibility with increasing the reciprocal of the slenderness ratio.

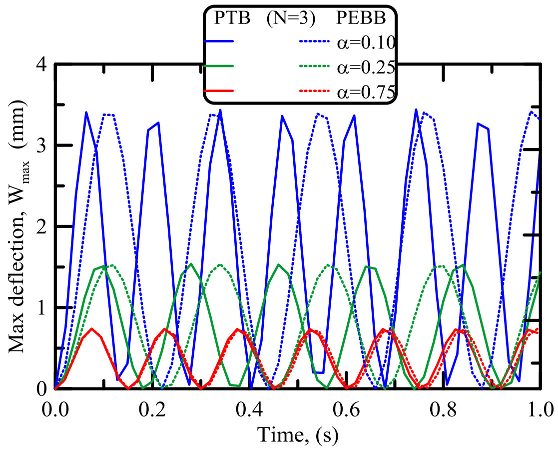

Fig. 17 Variation of W_{max} with the filling ratio for slender PBs with %R = 2% at N = 3

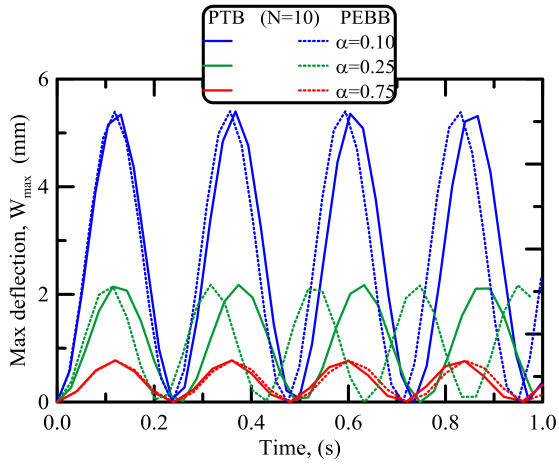

Fig. 19 Variation of W_{max} with the filling ratio for slender PBs with %R = 2% at N = 10

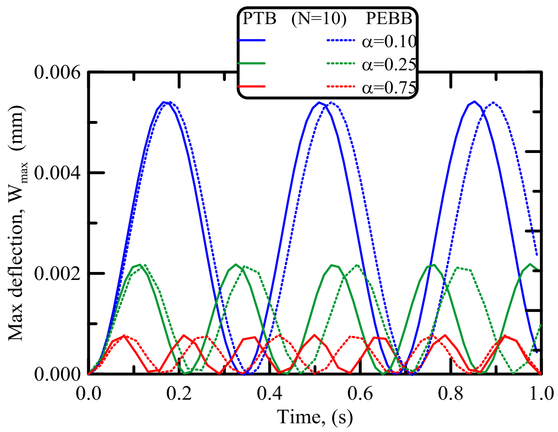

Fig. 18 Variation of W_{max} with the filling ratio for stocky PBs with %R = 20 % at N = 10

6. Conclusions

Vibration behaviors of perforated Euler Bernoulli and Timoshenko beams are investigated analytically. Due to the shear deformation effects associated with perforation process, conditions that govern employing the EBBT to analyze the dynamic behavior of perforated beams are determined. The validity of the developed analytical technique is checked by comparing the obtained results for both solid and perforated beams with the corresponding analytical and numerical results and good agreement is noticed. To investigate the effects of shear deformation pronounced in perforated beams, both Stocky and slender beams are analyzed. Effects of the beam filling ratio and the number of holes on the free and forced vibration characteristics of perforated beams are illustrated. The following concluding remarks are detected:

- If the resonant frequencies are the major factor in designing the perforated beam structures, EBBT can be employed to accurately predict the resonant frequencies of very slender beams with a reciprocal slenderness ratio of 1% and for filling ratio greater than 0.3. On the other hand, if the global transient response is the major interest, EBBT can efficiently predict the transient time response of perforated beams with any value of the reciprocal of the slenderness ratio and for any range of filling ratio and number of holes.
- The resonant frequencies are increased with increasing the beam filling ratio due to the decreasing in the hole size which increases the system equivalent stiffness. On the other side, these resonant frequencies are decreased with increasing the number of holes due to the decrease in the equivalent stiffness of the system.
- The perforated beam filling ratio as well as the number of holes is significantly affect the maximum transvers vibration amplitude of the forced vibration time response. The amplitude of the forced vibration response decreases with increasing the filling ratio due to the decrease in the system flexibility while it is increases with increasing the number of holes due to decreasing the system equivalent stiffness.
- The reciprocal of the slenderness ratio, %R, highly affects the forced vibration time response of both PEBB and PTB. Increasing the value of %R results in large drop in the forced vibration amplitudes.

References

Abdelbari, S., Amar, L.H.H., Kaci, A. and Tounsi, A. (2018), "Single variable shear deformation model for bending analysis of thick beams", *Struct. Eng. Mech., Int. J.*, **67**(3), 291-300. http://dx.doi.org/10.12989/sem.2018.67.3.291

Adhikary, S.D., Li, B. and Fujikake, K. (2012), "Dynamic behavior of reinforced concrete beams under varying rates of concentrated loading", *Int. J. Impact Eng.*, **47**, 24-38.

Bebiano, R., Calçada, R., Camotim, D. and Silvestre, N. (2017), "Dynamic analysis of high-speed railway bridge decks using generalised beam theory", *Thin-Wall. Struct.res*, **114**, 22-31.

Berggren, S.A., Lukkassen, D., Meidell, A. and Simula, L. (2003), "Some methods for calculating stiffness properties of periodic structures", *Applica. Math.*, **48**(2), 97-110.

Bennai, R., Atmane, H.A. and Tounsi, A. (2015), "A new higher-order shear and normal deformation theory for functionally graded sandwich beams", *Steel Compos. Struct., Int. J.*, **19**(3), 521-546. http://dx.doi.org/10.12989/scs.2015.19.3.521

Bourada, M., Kaci, A., Houari, M.S.A. and Tounsi, A. (2015), "A new simple shear and normal deformations theory for functionally graded beams", *Steel Compos. Struct., Int. J.*, **18**(2), 409-423. http://dx.doi.org/10.12989/scs.2015.18.2.409

Bouremana, M., Houari, M.S.A., Tounsi, A., Kaci, A. and Bedia, E.A.A. (2013), "A new first shear deformation beam theory based on neutral surface position for functionally graded beams", *Steel Compos. Struct., Int. J.*, **15**(5), 467-479. http://dx.doi.org/10.12989/scs.2013.15.5.467

Cortés, C., Osorno, M., Uribe, D., Steeb, H., Ruiz-Salguero, O., Barandiarán, I. and Flórez, J. (2019), "Geometry simplification of open-cell porous materials for elastic deformation FEA", *Eng. Comput.*, **35**, 257-276.

De Pasquale, G., Veijola, T. and Somà, A. (2009), "Modelling and validation of air damping in perforated gold and silicon MEMS plates", *J. Micromech. Microeng.*, **20**(1), 015010.

Driz, H., Benchohra, M., Bakora, A., Benachour, A., Tounsi, A. and Bedia, E.A.A. (2018), "A new and simple HSDT for isotropic and functionally graded sandwich plates", *Steel Compos. Struct., Int. J.*, **26**(4), 387-405. http://dx.doi.org/10.12989/scs.2018.26.4.387

Eltaher, M.A., Emam, S.A. and Mahmoud, F.F. (2012), "Free vibration analysis of functionally graded size-dependent nanobeams", *Appl. Math. Computat.*, **218**(14), 7406-7420.

Eltaher, M.A., Alshorbagy, A.E. and Mahmoud, F.F. (2013), "Vibration analysis of Euler–Bernoulli nanobeams by using finite element method", *Appl. Math. Model.*, **37**(7), 4787-4797.

Eltaher, M.A., Abdelrahman, A.A., Al-Nabawy, A., Khater, M. and Mansour, A. (2014a), "Vibration of nonlinear graduation of nano-Timoshenko beam considering the neutral axis position", *Appl. Math. Computat.*, **235**, 512-529.

Eltaher, M.A., Hamed, M.A., Sadoun, A.M. and Mansour, A. (2014b), "Mechanical analysis of higher order gradient nanobeams", *Appl. Math. Computat.*, **229**, 260-272.

Eltaher, M.A., Khater, M.E., Park, S., Abdel-Rahman, E. and Yavuz, M. (2016), "On the static stability of nonlocal nanobeams using higher-order beam theories", *Adv. Nano Res., Int. J.*, **4**(1), 51-64. 10.12989/anr.2016.4.1.051

Eltaher, M.A., Abdraboh, A.M. and Almitani, K.H. (2018a), "Resonance frequencies of size dependent perforated nonlocal nanobeam", *Microsyst. Technol.*, **24**(9), 3925-3937.

Eltaher, M.A., Kabeel, A.M., Almitani, K.H. and Abdraboh, A.M. (2018b), "Static bending and buckling of perforated nonlocal size-dependent nanobeams", *Microsyst. Technol.*, **24**(12), 4881-4893.

Ghayesh, M.H., Farokhi, H., Gholipour, A. and Tavallaeinejad, M. (2017), "Nonlinear bending and forced vibrations of axially functionally graded tapered microbeams", *Int. J. Eng. Sci.*, **120**, 51-62.

Greco, A., Pluchino, A., Caddemi, S., Caliò, I. and Cannizzaro, P. (2019), "On profile reconstruction of Euler–Bernoulli beams by means of an energy based genetic algorithm", *Eng. Comput.*

Guha, K., Kumar, M., Agarwal, S. and Baishya, S. (2015), "A modified capacitance model of RF MEMS shunt switch incorporating fringing field effects of perforated beam", *Solid-State Electronics*, **114**, 35-42.

Guha, K., Laskar, N.M., Gogoi, H.J., Borah, A.K., Baishnab, K.L. and Baishya, S. (2017), "Novel analytical model for optimizing the pull-in voltage in a flexured MEMS switch incorporating beam perforation effect", *Solid-State Electronics*, **137**, 85-94.

Guha, K., Laskar, N.M., Gogoi, H.J., Baishnab, K.L. and Rao, K.S. (2018), "A new analytical model for switching time of a perforated MEMS switch", *Microsyst. Technol.*, 1-10.

Gul, U., Aydogdu, M. and Karacam, F. (2019), "Dynamics of a functionally graded Timoshenko beam considering new spectrums", *Compos. Struct.*, **207**, 273-291.

Han, S.M., Benaroya, H. and Wei, T. (1999), "Dynamics of transversely vibrating beams using four engineering theories", *J. Sound Vib.*, **225**(5), 935-988.

Heidari, A., Keikha, R., Haghighi, M.S. and Hosseinabadi, H. (2018), "Numerical study for vibration response of concrete beams reinforced by nanoparticles", *Struct. Eng. Mech., Int. J.*, **67**(3), 311-316. https://doi.org/10.12989/sem.2018.67.3.311

Hopcroft, M.A., Nix, W.D. and Kenny, T.W. (2010), "What is the Young's modulus of silicon?", *J. Microelectromech. Syst.*, **19**, 229-238.

Inman, D.J. (2014), *Engineering Vibration*, (4th ed.), Pearson, Pearson Education.

Jeong, K.H. and Amabili, M. (2006), "Bending vibration of perforated beams in contact with a liquid", *J. Sound Vib.*, **298**(1-2), 404-419.

Katariya, P.V. and Panda, S.K. (2018), "Numerical evaluation of transient deflection and frequency responses of sandwich shell structure using higher order theory and different mechanical loadings", *Eng. Comput.*, 1-18.

Kerid, R., Bourouina, H., Yahiaoui, R., Bounekhla, M. and Aissat, A. (2019), "Magnetic field effect on nonlocal resonance frequencies of structure-based filter with periodic square holes network", *Physica E: Low-dimensional Syst. Nanostruct.*, **105**, 83-89.

Kim, J.H., Jeon, J.H., Park, J.S., Seo, H.D., Ahn, H.J. and Lee, J.M. (2015), "Effect of reinforcement on buckling and ultimate strength of perforated plates", *Int. J. Mech. Sci.*, **92**, 194-205.

Kim, T., Park, I. and Lee, U. (2017), "Forced vibration of a Timoshenko beam subjected to stationary and moving loads using the modal analysis method", *Shock Vib.*

Lee, Y.Y. (2016), "The effect of leakage on the sound absorption of a nonlinear perforated panel backed by a cavity", *Int. J. Mech. Sci.*, **107**, 242-252.

Luschi, L. and Pieri, F. (2012), "A simple analytical model for the resonance frequency of perforated beams", *Procedia Eng.*, **47**, 1093-1096.

Luschi, L. and Pieri, F. (2014), "An analytical model for the determination of resonance frequencies of perforated beams" *J. Micromech. Microeng.*, **24**(5), 055004.

Luschi, L. and Pieri, F. (2016), "An analytical model for the resonance frequency of square perforated Lamé-mode resonators", *Sensors Actuators B: Chem.*, **222**, 1233-1239.

Nikkhoo, A., Rofooei, F.R. and Shadnam, M.R. (2007), "Dynamic behavior and modal control of beams under moving mass", *J. Sound Vib.*, **306**(3-5), 712-724.

Pedersen, M., Olthuis, W. and Bergveld, P. (1996), "On the mechanical behaviour of thin perforated plates and their application in silicon condenser microphones", *Sensors Actuators A: Phys.*, **54**(1-3), 499-504.

Rajasekaran, S. (2018), "Analysis of axially functionally graded nano-tapered Timoshenko beams by element-based Bernstein pseudospectral collocation (EBBPC)", *Eng. Comput.*, **34**(3), 543-563.

Rao, S.S. (2007), *Vibration of Continuous Systems*, John Wiley & Sons.

Rouhi, H., Ebrahimi, F., Ansari, R. and Torabi, J. (2019), "Nonlinear free and forced vibration analysis of Timoshenko nanobeams based on Mindlin's second strain gradient theory", *Eur. J. Mech.-A/Solids*, **73**, 268-281.

Shafiei, N. and She, G.L. (2018), "On vibration of functionally graded nano-tubes in the thermal environment", *Int. J. Eng. Sci.*, **133**, 84-98.

She, G.L., Yuan, F.G. and Ren, Y.R. (2017), "Thermal buckling and post-buckling analysis of functionally graded beams based on a general higher-order shear deformation theory", *Appl. Math. Model.*, **47**, 340-357.

She, G.L., Ren, Y.R., Xiao, W.S. and Liu, H.B. (2018a), "Study on thermal buckling and post-buckling behaviors of FGM tubes resting on elastic foundations", *Struct. Eng. Mech., Int. J.*, **66**(6), 729-736.

She, G.L., Yan, K.M., Zhang, Y.L., Liu, H.B. and Ren, Y.R. (2018b), "Wave propagation of functionally graded porous nanobeams based on non-local strain gradient theory", *Eur. Phys. J. Plus*, **133**(9), 368.

Sınır, S., Çevik, M. and Sınır, B.G. (2018), "Nonlinear free and forced vibration analyses of axially functionally graded Euler-Bernoulli beams with non-uniform cross-section", *Compos. Part B: Eng.*, **148**, 123-131.

Song, Y., Kim, T. and Lee, U. (2016), "Vibration of a beam subjected to a moving force: Frequency-domain spectral element modeling and analysis", *Int. J. Mech. Sci.*, **113**, 162-174.

Tekili, S., Khadri, Y., Merzoug, B., Daya, E.M. and Daouadji, A. (2017), "Free and Forced Vibration of Beams Strengthened by Composite Coats Subjected to Moving Loads", *Mech. Compos. Mater.*, **52**(6), 789-798.

Thai, S., Thai, H.T., Vo, T.P. and Patel, V.I. (2018), "A simple shear deformation theory for nonlocal beams", *Compos. Struct.*, **183**, 262-270.

Tu, W.H., Chu, W.C., Lee, C.K., Chang, P.Z. and Hu, Y.C. (2013), "Effects of etching holes on complementary metal oxide semiconductor–microelectromechanical systems capacitive structure", *J. Intel. Mater. Syst. Struct.*, **24**(3), 310-317.

CC